

# Probing the flavor-specific scalar mediator for the muon $(g - 2)$ deviation, the proton radius puzzle and the light dark matter production

---

Bin Zhu,<sup>1,2</sup> Xuwen Liu<sup>1</sup>

<sup>1</sup>*Department of Physics, Yantai University, Yantai 264005, China*

<sup>2</sup>*Department of Physics, Chung-Ang University, Seoul 06974, Korea*

*E-mail:* [zhubin@mail.nankai.edu.cn](mailto:zhubin@mail.nankai.edu.cn), [xuwenliu@ytu.edu.cn](mailto:xuwenliu@ytu.edu.cn)

**ABSTRACT:** Flavor-specific scalar bosons exist in various proposed extensions of the Standard Model and couple to a single generation of fermion through a global flavor symmetry breaking mechanism. Given this strategy, we propose a MeV flavor-specific scalar model in dimension-5 operator series, explaining muon  $g-2$  anomaly and proton radius puzzle through the coupling with muon and down-quark simultaneously. The framework is consistent with the null result of high-intensity searches. Specifically, the E137 and supernova constraints for muon couplings become almost vanishing by including the contribution of down-quark interaction. We also investigate the searches for mediator and dark matter and the resulting constraints on viable parameter space such as nuclear physics constraints, direct detection for light boosted dark matter, and possible CMB constraints. Light dark matter production has two additional modifications compared with conventional one: bound state formation and early kinetic equilibrium decoupling. We further investigate the implications of these effects on the relic density of light dark matter.

---

## Contents

<b>1</b>	<b>Introduction</b>	<b>1</b>
<b>2</b>	<b>Muon-philic and down-philic scalar mediator</b>	<b>3</b>
<b>3</b>	<b>The muon (g-2), proton charge radius and constraints</b>	<b>4</b>
<b>4</b>	<b>Dark matter production</b>	<b>9</b>
<b>5</b>	<b>Conclusion</b>	<b>12</b>

---

## 1 Introduction

Muon g-2 is an extremely sensitive probe for new physics models. Recently the Fermilab released the first results of the muon g-2 experiment, which confirms the Brookhaven results on the long-standing anomaly of the anomalous magnetic moment of the muon, namely the discrepancy between the experimental results [1, 2] and theoretical predictions [3–7]. The new result further strengthens the significance to be about  $4.2 \sigma$  deviation [8],

$$\Delta a_\mu = a_\mu^{\text{exp}} - a_\mu^{\text{th}} = (2.51 \pm 0.59) \times 10^{-9} . \quad (1.1)$$

The hypothesis of a muonic force mediated by a scalar or vector boson in the MeV range could explain this anomaly. In addition, laser spectroscopy of muonic hydrogen [9] yielded a proton charge radius that does not agree, at about  $5\sigma$  level, with the value obtained from electron-proton scattering and electron hydrogen spectroscopy [10, 11]. This discrepancy is the proton radius puzzle. It is another basic motivation for muonic force. Even though some recent data on  $ep$  scattering [12] and H spectroscopy [13, 14] remove discrepancy with muonic hydrogen results to some extent, a few recent experimental collaborations [15, 16] have reported  $r_p$  values that persistently agree with the CODATA 2014  $r_p$  value, which leaves the proton charge radius puzzle ameliorated but not conclusively gone,

$$r_p^{(e)} = 0.8751 \pm 0.0061 \text{ fm}, \quad r_p^{(\mu)} = 0.84087 \pm 0.00039 \text{ fm}. \quad (1.2)$$

The existence of new force [17–24] mediated by a low-mass particle with very weak coupling to SM particles is the main target at the intensity frontiers [25] and nuclear physics. The resulting bounds on the parameters are illustrated in the context of a flavor-specific scalar model [26–28]. We suggest that flavor-specific scalar  $\phi$  may be the relaxation process that resolves both discrepancies at MeV scale. Generally, the scalar mediator model is Higgs portal interaction [29]. However, we adapt the effective field theory approach,  $d = 5$  operators,

where mediator  $\phi$  couples to muon and down-quark simultaneously. Higher-dimensional operators are suppressed by UV cut-off  $M$ . The spurion analysis allows a mediator to break flavor universality and couple to a single generation of fermions. Therefore, we can investigate the multi-scale problems of relating the high precision measurements with muons in this model-independent approach.

For MeV-scale mediator to survive across many beam dump experiments such as E137 [30], we require the mediator decays into photons in both muon and down-quark loops. The coupling  $\phi F^{\mu\nu} F_{\mu\nu}$  [31, 32] from muon and down-quark loop leading to supernova cooling and E137 are softened by the existence of quark coupling. It shows that supernova cooling simulation rules out a mediator lighter than one MeV. The associated rare Kaon decay constraints in E949 [33] are vanishing when the mediator couples to down-quark rather than up-quark.

From a perspective of dark matter, the calculations on  $\Delta N_{\text{eff}}$  show that dark matter is heavier than MeV. We will discuss the implication of light dark matter relic density produced by the  $\chi\chi \rightarrow \phi\phi$  process together with Sommerfeld correction. Even though the annihilation process is P-wave, the corresponding bound state formation cross-section remains s-wave and introduces CMB constraints. In addition, the direct detection loses sensitivity to the light-dark matter since it produces not efficient recoil energy in the noble liquid detector. While some astrophysical sources can boost light dark matter into a fast-moving component that recovered detector sensitivity. For example, cosmic-ray can scatter with dark matter in the halo [34, 35]. The resulting dark matter gets sufficient kinetic energy to overcome the threshold of the detector. Therefore, this mechanism can constrain our parameter space of the dark sector.

This paper is structured as follows: we begin in section 2 by presenting the flavor-specific scalar model. In section 3, we provide the explanations of both Muon  $(g - 2)$  and proton charge radius anomalies. In addition, we analyze the constraints on the parameter space from nuclear physics and various experimental data. In section 4, we investigate the DM production. As a proof of principle of the mass hierarchy  $m_\phi < m_\chi$  from  $\Delta N_{\text{eff}}$  constraint, we will then apply it for calculating relic density of dark matter. Since the cross-section of direct annihilation into muons and photons is smaller than that into mediators, the relic density calculation belongs to the secluded dark matter scenario  $\chi\chi \rightarrow \phi\phi$  [23]. However, there are two possible modifications of the secluded dark matter. The underlying assumption on kinetic equilibrium relies upon the elastic scattering process between dark matter and mediator. If it not sufficient, the early kinetic decoupling might happen and affect the relic density. Another possible modification comes from the light mediator, which allows for the existence of the bound state in the cosmological evolution of dark matter. Its existence also affects the relic density. We will investigate it in detail in section 4. Finally, the last section is devoted to our conclusion.

## 2 Muon-philic and down-philic scalar mediator

Identifying the dark sector has become mainstream in physics society. There is a consensus that dark matter is a sub-GeV particle with a mediator communicating dark matter and Standard Model particles. Even though, which types of mediators hypothesis remain to be verified, we prefer the mediator a real scalar because other types of a mediator cannot account for the proton radius puzzle [36]. Therefore, we describe the dark sector-SM interaction through the model-independent dimension-5 operators

$$-\mathcal{L}_{d=5} = \frac{C_u^{ij}}{M} \phi H^c \bar{Q}_L^i u_R^j + \frac{C_d^{ij}}{M} \phi H \bar{Q}_L^i d_R^j + \frac{C_e^{ij}}{M} \phi H E_L^i e_R^j + h.c. \quad (2.1)$$

Indeed there are other dimension-5 operators i.e.  $\partial_\mu \phi \bar{q} \gamma^\mu q$ . They are equivalent to equation 2.1 after a field redefinition. Furthermore the mediator  $\phi$  could couple to neutrino via  $C_\nu/M^2 \phi (HL)^2$ . It is a dimension-6 operator and thus becomes negligible unless an unnatural hierarchy of Wilson coefficients holds such as  $C_\nu \sim 10^{10} C_q$ .

We will discuss the implication of such operators in equation 2.1 for low energy phenomenology such as the muon ( $g-2$ ) and the proton radius puzzle. Here  $i$  and  $j$  stand for generation indices of quarks and leptons. Thus the Wilson coefficients  $C_{u,d,e}$  are generic  $3 \times 3$  matrix. From a perspective of flavor violation constraint, some assumptions on global symmetry breaking of flavor structure are imposed. For example, a breaking  $U(3)_Q \times U(3)_D \rightarrow U(1)_d \times U(2)_L \times U(2)_R$  can assure only  $C_d^{11}$  is non-vanishing for quark Wilson coefficient  $C_{u,d}$ . Employing symmetry breaking pattern for leptons can yield a residue  $U(1)_\mu$ . In that sense only  $C_e^{22}$  is non-vanishing. We should mention that our analysis is just a hypothesis that resorts to a UV completion. For example, the simplest UV completion is to take SUSY breaking spurion-sgoldstino [37] as force carrier.

After electroweak symmetry breaking, the relevant portal interaction with SM from dimension-5 operator 2.1 becomes

$$-\mathcal{L}_{\text{Portal}} = g_d \phi \bar{d}_L d_R + g_\mu \phi \bar{\mu}_L \mu_R + h.c., \quad (2.2)$$

where  $g_d = C_d^{11} v/M$ ,  $g_\mu = C_e^{22} v/M$ . Despite other approaches of MeV force scenario, the novelty of our model is that proton and neutron couplings are fixed by  $g_d$  uniquely

$$g_p = 0.039 g_d \frac{m_p}{m_d}, \quad g_n = 0.049 g_d \frac{m_n}{m_d}. \quad (2.3)$$

We take the dark matter to be Dirac fermion for simplicity and couples to mediator  $\phi$  in the following interaction

$$\mathcal{L}_{\text{Dark}} = i \bar{\chi} \gamma^\mu \partial_\mu \chi - m_\chi \bar{\chi} \chi - g_\chi \bar{\chi} \chi \phi \quad (2.4)$$

In the absence of additional interactions and assume dark matter is heavier than mediator, for  $m_\chi > m_\phi > 2m_\mu$ , the dominant decay is  $\phi \rightarrow \mu^+ \mu^-$  with partial width

$$\Gamma_{\phi \rightarrow \mu^+ \mu^-} = \frac{g_\mu^2 m_\phi}{8\pi} \left(1 - \frac{4m_\mu^2}{m_\phi^2}\right)^{3/2}, \quad (2.5)$$

The beam dump experiment is also sensitive to decay channel into pions when  $m_\phi > 2m_\pi$ . This channel is not absent, because the proton radius puzzle favors a MeV-scale mediator. For  $m_\phi < 2m_\mu$ , the dominant channel is  $\phi \rightarrow \gamma\gamma$  through a muon and down quark loop,

$$\Gamma_{\phi \rightarrow \gamma\gamma} = \frac{\alpha^2 g_\mu^2 m_\phi^3}{144\pi^3 m_\mu^2} \left| F_{1/2} \left( \frac{4m_\mu^2}{m_\phi^2} \right) \right|^2 + \frac{\alpha^2 N_c^2 Q_d^4 g_d^2 m_\phi^3}{144\pi^3 m_d^2} \left| F_{1/2} \left( \frac{4m_d^2}{m_\phi^2} \right) \right|^2, \quad (2.6)$$

where the loop function is

$$F_{1/2}(\tau) = \frac{3\tau}{2} \left[ 1 + (1 - \tau) \left( \sin^{-1} \frac{1}{\sqrt{\tau}} \right)^2 \right]. \quad (2.7)$$

The visible decay final state  $\phi \rightarrow \gamma\gamma, \mu\mu$  plays a crucial role in increasing the projection for the NA62 [38] search for  $K \rightarrow \mu\nu\phi$ . While most of the available parameter space for muonic force is excluded by E137. However, our model has additional coupling with down-quark, we can shift the the excluded region for muon coupling to  $10^{-2}$ , that recovers the room for explaining the muon  $g - 2$  discrepancy.

### 3 The muon (g-2), proton charge radius and constraints

The scalar mediator provides an additional contribution to the anomalous magnetic moment of the muon at one loop. The shift due to the vertex correction is [39]

$$\Delta a_\mu = \frac{g_\mu^2}{8\pi^2} \int_0^1 dz \frac{(1-z)^2(1+z)}{(1-z)^2 + (m_\phi/m_\mu)^2 z}. \quad (3.1)$$

Utilizing this new effect, we filled up the discrepancy between the experimental data and theoretical prediction within 2 standard deviations, shown by blue color in Figs. 1 and 2. The Favored values of muonic coupling  $g_\mu$  are around  $10^{-4}$ . It is easy to find that the future NA62 projection [28] can exclude or confirm the model, labeled by the magenta dashed line.

In Fig. 2, we set  $g_\mu = 3.7 \times 10^{-4}$  according to allowed parameter space in Fig. 1, which also satisfies the experimental constraints as will be discussed in the following. The mediator mass is solved to be 1.8 MeV to obtain the central value of  $\Delta a_\mu$ , shown by the blue vertical line. Also, the range of  $m_\phi > 20$  MeV is out of the data error at the time.

Spectroscopy in Hydrogen-like atoms can be changed by the finite-sized proton, which induces the Lamb to shift  $\Delta E_{\text{Lamb}}$  between the 2S and 2P energy levels. Then the measurements of the Lamb shift can deduce the proton charge radius. The existence of the new scalar causes an extra contribution to the Lamb shift in muonic hydrogen and could be account for

the deviation of the proton size measurements. Usually, the Yukawa potential provides a new attractive force that modifies the  $\mu - p$  system,

$$V(r) = -\frac{1}{4\pi} g_\mu g_p e^{-m_\phi r} / r. \quad (3.2)$$

As a result, the additional contribution to the Lamb shift  $\Delta E_{\text{Lamb}}$  in muonic hydrogen is given by [40–43]

$$\delta E_{\text{Lamb}}^{\ell\text{N}} = \langle 2S | V(r) | 2S \rangle - \langle 2P | V(r) | 2P \rangle \quad (3.3)$$

$$= -\frac{g_\mu}{8\pi a_{\ell\text{N}}} [Zg_p + (A - Z)g_n] f(a_{\ell\text{N}} m_\phi), \quad (3.4)$$

where  $f(x) = x^2/(1+x)^4$ , with  $a_{\ell\text{N}} = (Z\alpha m_{\ell\text{N}})^{-1}$  the Bohr radius and  $m_{\ell\text{N}}$  is the reduced mass of the lepton-nucleus system.  $A$  and  $Z$  are atom number and the proton number in an atom. In the following, we use

$$\delta E_{\text{Lamb}}^{\mu\text{H}} = -0.307(56) \text{ meV} \quad (3.5)$$

within two standard deviations to be fitted in our model. By employing this energy shift we can determine both  $g_\mu$  and  $g_d$  as functions of  $m_\phi$ . The red shaded regions in Figs. 1 and 2 show the central value and the error band of  $\delta E_{\text{Lamb}}^{\mu\text{H}}$ . To demonstrate the results explicitly, in Fig. 1 we set  $g_d = 8 \times 10^{-5}$  which is allowed by various experimental constraints. In Figs. 1 and 2, we find that there is room for accommodating both anomalies simultaneously, and the mediator mass around 1.2 MeV is favored with  $g_\mu = 4 \times 10^{-4}$ . As will be seen in the following, after considering the constraints, the viable parameter space is severely limited, especially by the supernova constraints and nuclear physics. Future experiments such as NA62 and direct detection can probe our model.

There are a variety of constraints from both nuclear physics and experiments in the wide range.

- Cooling of supernova (SN 1987A) constraints for muon coupling  $g_\mu$

Most axion couplings such as the electrons, photons are highly constrained by the stellar cooling process when axion mass is below 1 MeV. The role of axion-muon coupling in a supernova can also have constraints in Ref. [44]. The high temperature of axion production and electron degeneracy give rise to room for the abundance of muons. Therefore its falling in temperature after simulation sheds lights on axion-muon couplings as  $g_{a\mu} < 10^{-8.1} \text{ GeV}^{-1}$ . We can interpret this constraint for our muonic force mediator  $\phi$ ,

$$g_\mu < 1.67 \times 10^{-9}, \quad \text{when } m_\phi < 1 \text{ MeV}. \quad (3.6)$$

The loop-induced coupling between mediator and photon is constrained by supernova cooling too [31, 32]. If there is only a muon loop, supernova cooling excludes the model easily. However, the existence of the down quark loop reduces the bound of  $g_\mu$  to be smaller than our threshold  $10^{-5}$ . Therefore, this constraint becomes vanishing.

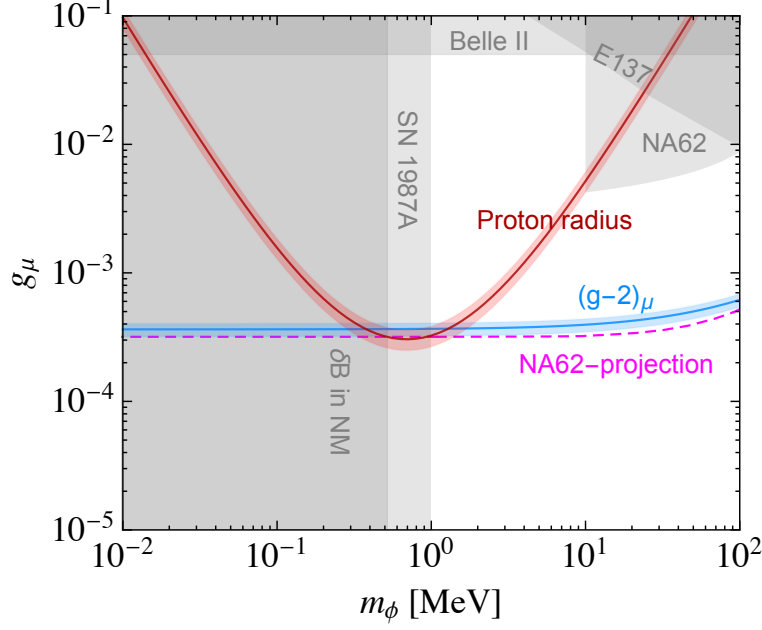


**Figure 1:** Muon  $(g-2)$  anomaly, proton radius puzzle and experimental constraints, plotted as functions of the scalar mass  $m_\phi$  and coupling  $g_\mu$ . Here we set  $g_d = 8 \times 10^{-5}$ . Blue: region that can explain the  $(g-2)_\mu$  anomaly in  $2\sigma$  deviation. The blue line is the measured central value of the  $\Delta a_\mu$  data. Red: region in which can address the proton radius puzzle. The solid line corresponds to the central value in equation 3.5, while the shaded regions include the  $2\sigma$  compatible values. Gray: excluded regions by nucleon binding energy in nuclear matter (indicated with “ $\delta B$  in NM”), by cooling of supernova (“SN 1987A”), by the Belle II experiments which constraints on  $\mu^+\mu^-$  final state with missing ET (denoted as “Belle II”), by NA62 on Br ( $K^+ \rightarrow \mu^+ + \text{invisible}$ ) at 90% C.L. and by E137. The magenta dashed line corresponds to the NA62 projection for  $K^+ \rightarrow \mu^+ + \text{invisible}$  searching.

- Nucleon Binding Energy in (N=Z) Nuclear Matter ( $\delta B$  in NM)

The scalar coupling to the nucleons provides additional contributions to the nucleon binding energy in (N=Z) nuclear matter. The change in nucleon binding energy in infinite nuclear matter is [36]

$$\delta B = \frac{(g_p + g_n)^2 \rho}{4m_\phi^2}, \quad (3.7)$$

where  $\rho \approx 0.08 \text{ fm}^{-3}$  is the nucleon density. The extra contribution is less than 1 MeV to avoid conflicts with nuclear physics. It turns out that the constraints on the mediator mass  $m_\phi$  and coupling  $g_d$  are very strict. The mass range is limited to  $m_\phi > 4 \times 10^{-1}$  MeV, and also vast space of  $g_d$  is excluded as shown in black dashed line in Fig. 2.

- ${}^3\text{He}$ - ${}^3\text{H}$  binding energy difference ( ${}^3\text{He}$ - ${}^3\text{H}$ )

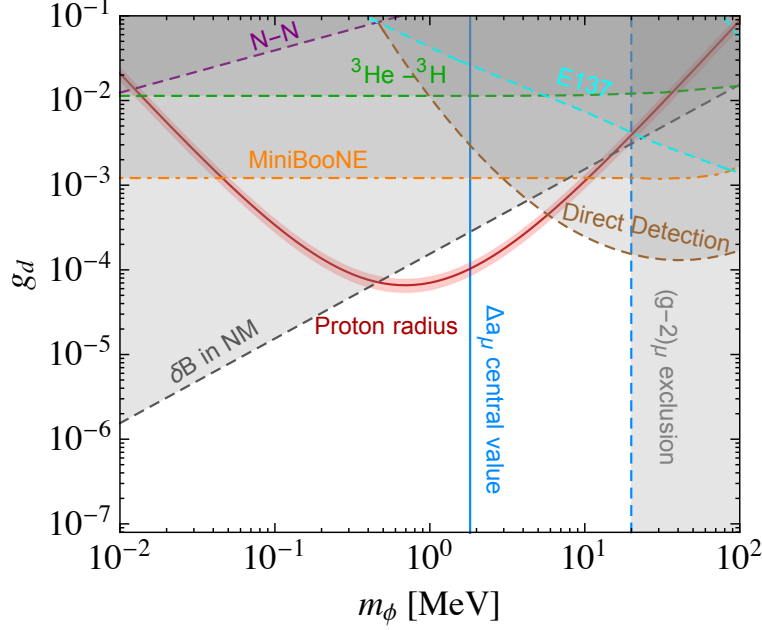


**Figure 2:** Muon  $(g - 2)$  anomaly, proton radius anomaly and experimental constraints, plotted as functions of the scalar mass  $m_\phi$  and coupling  $g_d$ . Here we set  $g_\mu = 3.7 \times 10^{-4}$ . Blue lines: The solid blue line is the measured central value of the  $\Delta a_\mu$  data. The dashed blue line is exclusion limits on scalar mass. Red: region in where can address the proton radius puzzle. The solid line corresponds to the central value, while the shaded regions include the  $2\sigma$  compatible values. Gray regions: excluded regions by various constraints. The black, green, purple, orange, cyan and brown dashed lines correspond to the constraints from nucleon binding energy in nuclear matter ( $\delta B$  in NM),  ${}^3\text{He}$ - ${}^3\text{H}$  binding energy difference ( ${}^3\text{He}$ - ${}^3\text{H}$ ), neutron- ${}^{208}\text{Pb}$  Scattering (N-N), MiniBooNE, E137 and the DM direct detection.

The binding energy difference between  ${}^3\text{He}$  and  ${}^3\text{H}$ , which is 763.76 keV, was composed of the contribution from Coulomb interaction and charge asymmetry of nuclear forces with high accuracy [45–49]. So non-SM effects from the scalar mediator  $\phi$  should be constrained which is set to be less than 30 keV [36]. The upper limits on  $g_d$  in our model are shown by the green dashed line in Fig. 2.

- Neutron-Nucleus Scattering (N-N)

The low energy neutron-nucleus scattering experiment with the nucleus  ${}^{208}\text{Pb}$  constrains the coupling between the scalar mediator and neutron  $g_N$  [50]. The constraints on coupling  $g_d$  in our model are the replacement  $g_N^2/4\pi \rightarrow 1/4\pi(1 - Z/A)g_n^2 + (Z/A)g_pg_n$ , where atomic mass  $A$  and the atomic number  $Z$  belong to the scattered nucleus. The purple dashed line in figure 2 stands for the upper limits on  $g_d$  as a function of the mediator mass  $m_\phi$ .



- MiniBooNE-Proton Beam Dumps

Fermilab Booster Neutrino Beam with 8 GeV probes the dark sector. Parameter space of dark photon is excluded between 5 MeV and 50 MeV [51]. The exclusion for coupling  $g_B$  maps into the coupling for  $g_d$ , where  $g_d$  larger than  $10^{-3}$  is ruled out. The boundary of the exclusion region is labeled by an orange dash-dotted line.

- Belle II constraints on  $\mu\mu$ +MET

Due to the coupling to muon, the mediator  $\phi$  can be produced at  $e^+e^-$  colliders in the process  $e^+e^- \rightarrow \mu^+\mu^-\phi$ , which subsequently becomes  $\mu^+\mu^- + \text{MET}$  final states. Recently, Belle II experiment performed the searches for the invisible decay of a  $Z'$  particle in the process  $e^+e^- \rightarrow \mu^+\mu^-Z' \rightarrow \mu^+\mu^- + \text{MET}$  using  $276 \text{ pb}^{-1}$  data [52], the null result put an upper bound on the muonic coupling which can be translated to be about  $g_\mu < 5 \times 10^{-2}$  at the region of  $m_\phi < 10^2 \text{ MeV}$  (see Fig. 1).

- Beam-dump Constraints

In a fixed-target environment, many neutral or charged mesons that can decay into photons and muons are produced. With suitable masses and interaction in our model, they can decay into dark matter instead. The constraint in E137 [30] at SLAC is tiny in our model due to the existence of down quark coupling. The invisible decay constraint  $K^+ \rightarrow \pi^+\nu\nu$  in E949 [33] is negligible since our mediator couples to down quark only. Up-type quark coupling appearing at one-loop can re-introduce the beam-dump experiment constraint. However, we mention that it tends to be less relevant in the recent experiment for its small couplings. Finally, the invisible decaying scenario can help us probe our model in NA62 via leptonic decay  $K \rightarrow \mu\nu\phi$ . It can be seen in Fig.1. The gray region labeled by NA62 is the excluded region from the following limits with existing data [53]

$$\text{BR}(K^+ \rightarrow \mu^+3\nu) < 10^{-6}. \quad (3.8)$$

- Xenon1T constraints

There is one method to detect our sub-GeV dark matter: accelerated dark matter. The typical example is the cosmic-ray boosted dark matter induced by proton coupling of  $\phi$ . The differential event rate is given explicitly

$$\frac{dR}{dE_R} = \int_{T_\chi(T_\chi^{z,\min})}^{\infty} dT_\chi \frac{d\sigma_{\chi N}}{dE_R} \frac{d\Phi_\chi}{dT_\chi}, \quad (3.9)$$

where  $T_\chi^{\min}$  is the minimal incoming dark matter kinetic energy to generate given recoil energy  $E_R$ .  $d\sigma_{\chi N}/dE_R$  is differential cross-section between dark matter and nucleons, and  $d\Phi_\chi/dT_\chi$  is differential dark matter flux. In terms of equation 3.9, we can recover the sensitivity of noble liquid detector on sub-GeV dark matter. The local population of cosmic-ray dark matter comes from collisions with the local interstellar (LIS). In terms of equation 3.9, the attenuated dark flux can provide a few different ways to constrain

dark matter-nucleon cross-section. The inclusion of the momentum transfer effect can enhance the event rate. We plot the exclusion limit in Fig. 2 with  $m_\phi = 0.1m_\chi$ . The upgrade of XenonNT and PandaX can push the exclusion line towards our model.

#### 4 Dark matter production

Since dark matter is heavier than 1.2 MeV mediator from the requirement of  $\Delta N_{\text{eff}}$  and BBN [54], the direct annihilation into muons or pions is suppressed relative to the secluded scenario  $\chi\chi \rightarrow \phi\phi$ ,

$$\sigma v_{\text{rel}} = \frac{3g_\chi^4 v_{\text{rel}}^2}{128\pi m_\chi^2}, \quad (4.1)$$

where  $g_\chi$  is the coupling between dark matter and mediator in equation 2.4. It is a P-wave process without CMB constraints. When Bohr radius of dark matter  $1/\alpha_\chi m_\chi$  is smaller than force radius  $1/m_\phi$ , Sommerfeld correction becomes inevitable:

$$\sigma v_{\text{rel}} = S_1(v_{\text{rel}}) \times (\sigma v_{\text{rel}})_0. \quad (4.2)$$

Under Hulthen approximation, the Sommerfeld enhancement is

$$S_1^H = \frac{(1 - \varepsilon_\phi \pi^2/6)^2 + 4\varepsilon_v^2}{(\varepsilon_\phi \pi^2/6)^2 + 4\varepsilon_v^2} S_0^H, \quad (4.3)$$

where  $\varepsilon_v = v_{\text{rel}}/2\alpha_\chi$ ,  $\varepsilon_\phi = m_\phi/(\alpha_\chi m_\chi)$ ,  $\alpha_\chi = g_\chi^2/4\pi$ , and  $S_0^H$  is s-wave Sommerfeld enhancement factor,

$$S_0^H = \frac{\pi}{\varepsilon_v} \frac{\sinh\left(\frac{2\pi\varepsilon_v}{\pi^2\varepsilon_\phi/6}\right)}{\cosh\left(\frac{2\pi\varepsilon_v}{\pi^2\varepsilon_\phi/6}\right) - \cos\left(2\pi\sqrt{\frac{1}{\pi^2\varepsilon_\phi/6} - \frac{\varepsilon_v^2}{(\pi^2\varepsilon_\phi/6)^2}}\right)}. \quad (4.4)$$

The calculation of the thermal freeze-out process resorts to solving the following Boltzmann equation

$$\dot{n} + 3Hn = -\langle\sigma v\rangle [n^2 - n_{\text{eq}}^2], \quad (4.5)$$

where  $\langle\sigma v\rangle$  is the thermal average of Sommerfeld corrected cross-section,  $n_{\text{eq}}$  corresponds to the dark matter number density in chemical equilibrium. It is easy to solve the Boltzmann equation 4.5 with yield  $Y_\chi = n_\chi/s$  as variable,

$$\frac{dY_\chi}{dx} = -\frac{\langle\sigma v\rangle}{H_{\text{eff}}x} s_{\text{SM}} (Y_\chi^2 - Y_{\text{eq}}^2). \quad (4.6)$$

Usually, the P-wave process is CMB-safe. However, as is discussed in [55], the bound state formation cross-section is S-wave which re-introduces CMB constraint. We can get an analytic solution of the monopole transition into the S-wave bound state

$$(\sigma v)_{n0}^M = \frac{2^6 \pi^3 \alpha_\chi^5 e^{-4n} (L_{n-1}^1(4n))^2}{9n^3 m_\chi m_\phi \sin^2(\pi \sqrt{\alpha_\chi m_\chi}/m_\phi)}. \quad (4.7)$$

The contribution in equation 4.7 is only significant for CMB rather than relic density. Since its leading-order contribution cancels with each other for the real scalar mediator. We refer to the solution of equation 4.6 as the minimal benchmark model of dark matter, which is denoted as Case-1. The variations of the minimal setup are classified as follows:

- (1) Why bound state formation is tiny compared with annihilation cross-section is that the real scalar mediator suffers from cancellation in the radiative formation of bound state. Given this fact, we consider the modification of Case-1, Case-2:

$$-\delta\mathcal{L} = c_\phi \phi^3 \quad (4.8)$$

which is the cubic self-interaction of the mediator. One-mediator emission of bound-state formation is thus non-vanishing [56–58],

$$\begin{aligned} \sigma_{\text{BSF}v_{\text{rel}}} &= \frac{\alpha_\chi^2}{\mu^2} \left( \frac{2c_\phi}{\mu\alpha_\chi^2} \right)^2 \sqrt{1 - \left( \frac{2m_\phi}{(\alpha_\chi^2 + v_{\text{rel}}^2)} \right)^2} S_0^H(\varepsilon_v, \varepsilon_\phi) \\ &\times \left( \frac{1/\varepsilon_\phi^2}{1 + 1/\varepsilon_\phi^2} \right)^2 \exp(-4/\varepsilon_\phi \operatorname{arccot}(1/\varepsilon_\phi)). \end{aligned} \quad (4.9)$$

In this case, the Boltzmann equation becomes coupled one where the bound state has its number density evolution. It can reduce to a single Boltzmann equation when we generalize the definition of the effective cross-section as

$$\langle \sigma_{\text{eff}} v_{\text{rel}} \rangle = \langle \sigma_{\text{ann}} v_{\text{rel}} \rangle + \langle \sigma_{\text{BSF}} v_{\text{rel}} \rangle_{\text{eff}}, \quad (4.10)$$

where the effective bound state formation scales as a function of decay, ionization of the bound state,

$$\langle \sigma_{\text{BSF}v_{\text{rel}}} \rangle_{\text{eff}} = \langle \sigma_{\text{BSF}v_{\text{rel}}} \rangle \times \left( \frac{\Gamma_{\text{dec}}}{\Gamma_{\text{dec}} + \Gamma_{\text{ion}}} \right), \quad (4.11)$$

with the decay and ionization of the bound state being

$$\Gamma_{\text{decay}} = \frac{0.01 |\Psi_{100}(0)|^2 g_\chi^8}{49152 \pi^6 m_\chi^2}, \quad \Gamma_{\text{ion}} = \langle \sigma_{\text{BSF}v_{\text{rel}}} \rangle \left( \frac{m_\chi T}{4\pi} \right)^{3/2} e^{-|E_B|/T} \quad (4.12)$$

It is easy to find that the cubic term  $c_\phi$  must be larger than  $10^4 \text{GeV}$  in our parameter space to affect relic density. However, such a large cubic coupling results in the challenge of CMB ionization and vacuum stability. Therefore Case-2 is not significant in our model. We leave the detailed analysis of Case-2 in the future study.

- (2) The derivation of equation 4.5 has an underlying assumption: kinetic equilibrium remains during chemical freeze-out. It becomes restrictive at some parameter space where elastic scattering between dark matter and mediator is not sufficient to retain kinetic equilibrium. It implies one must include additional variables to complete the equation. The convenient approach is to consider dark matter temperature  $T_\chi \equiv g_\chi / (3n_\chi) \int d^3p (2\pi)^{-3} (p^2/E) f_\chi$ . For the two variables system  $n_\chi, T_\chi$ , the coupled Boltzmann equation becomes

$$\begin{aligned} \frac{Y'}{Y} &= \frac{sY}{x\tilde{H}} \left[ \frac{Y_{\text{eq}}^2}{Y^2} \langle \sigma v \rangle_T - \langle \sigma v \rangle_{T_\chi} \right] \\ \frac{y'}{y} &= \frac{1}{x\tilde{H}} \langle C_{\text{el}} \rangle_2 + \frac{sY}{x\tilde{H}} [\langle \sigma v \rangle_{T_\chi} - \langle \sigma v \rangle_{2,T_\chi}] \\ &\quad + \frac{sY}{x\tilde{H}} \frac{Y_{\text{eq}}^2}{Y^2} \left[ \frac{y_{\text{eq}}}{y} \langle \sigma v \rangle_{2,T} - \langle \sigma v \rangle_T \right] + 2(1-w) \frac{H}{x\tilde{H}}, \end{aligned} \quad (4.13)$$

where  $Y(x) \equiv n/s, y(x) \equiv m_\chi T_\chi s^{-2/3}$ . We label this modification as Case-3.

For kinetic decoupling calculation, the temperature of dark matter is not usually the same as the temperature of the thermal bath, which becomes sizeable when the elastic scattering between dark matter and mediator is not efficient. The quantity to capture the elastic scattering process is  $C_{\text{el}}$  in the Fokker-Plank operator

$$C_{\text{el}} = \frac{E}{2} \gamma(T) \left[ TE \partial_p^2 + \left( 2T \frac{E}{p} + p + T \frac{p}{E} \right) \partial_p + 3 \right] f_\chi, \quad (4.14)$$

where  $\gamma$  is the momentum transfer rate,

$$\gamma = \frac{1}{3g_\chi m_\chi T} \int \frac{d^3k}{(2\pi)^3} g^\pm(\omega) [1 \mp g^\pm(\omega)] \int_{-4k_{\text{cm}}^2}^0 dt(-t) \frac{d\sigma}{dt} v. \quad (4.15)$$

In our model, the differential cross-section corresponds to  $\chi\phi \rightarrow \chi\phi$  process with  $(d\sigma/dt)v \equiv |\mathcal{M}|_{\chi f \leftrightarrow \chi f}^2 / (64\pi k \omega m_\chi^2)$ , which can be given explicitly,

$$\begin{aligned} \int dt(-t) d\sigma/dt v &= \frac{1}{3(m_\phi^2 + 2\omega m_\chi)^2} \times \\ &\quad \frac{\sum_i (4k^2 m_\chi^2)^{i-1} C_i}{\left( m_\phi^4 + \left( 4(k-\omega)(k+\omega) + m_\phi^2 \right) m_\chi^2 - 2\omega m_\chi^3 \right) \left( m_\phi^2 + m_\chi (2\omega + m_\chi) \right)^3 }, \end{aligned} \quad (4.16)$$

where  $C_i$  is just combination of  $m_\chi, m_\phi$  and  $\omega$ :

$$\begin{aligned} C_1 &= -3 \left( \log [-m_\phi^2 + 2\omega m_\chi] - \log \left[ -m_\phi^2 + 2m_\chi \left( \omega - \frac{2k^2 m_\chi}{m_\phi^2 + 2\omega m_\chi + m_\chi^2} \right) \right] \right) \\ &\quad \times (m_\phi^2 + 2\omega m_\chi) (m_\phi^6 - 2m_\phi^4 m_\chi^2 - m_\phi^2 m_\chi^2 (\omega^2 + 4m_\chi (3\omega + m_\chi)) \\ &\quad - 2\omega m_\chi^3 (\omega^2 - 4m_\chi (2\omega + 3m_\chi))), \end{aligned} \quad (4.17)$$

$$\begin{aligned}
C_2 = & -16k^6 m_\chi^6 (m_\phi^2 + 2\omega m_\chi) + 6k^2 m_\chi^2 (m_\phi^2 + m_\chi(2\omega + m_\chi))^2 \\
& \times (-m_\phi^6 + 2m_\phi^4 m_\chi(m_\chi - 2\omega) + 2\omega m_\chi^3(-5\omega^2 + 8\omega m_\chi + 12m_\chi^2) \\
& + m_\phi^2 m_\chi^2(-7\omega^2 + 20m_\chi(\omega + m_\chi))) + 8k^4 m_\chi^4 (m_\phi^2 + m_\chi(2\omega + m_\chi)) \\
& \times (m_\phi^4 + 6m_\phi^2 m_\chi(\omega + m_\chi) + m_\chi^2(11\omega^2 + 12m_\chi(2\omega + m_\chi))) \\
& - 3(m_\phi^2 + 2\omega m_\chi)(m_\phi^2 + m_\chi(2\omega + m_\chi))^3 (m_\phi^6 - 2m_\phi^4 m_\chi^2 - m_\phi^2 m_\chi^2 \\
& \times (\omega^2 + 4m_\chi(3\omega + m_\chi)) - 2\omega m_\chi^3(\omega^2 - 4m_\chi(2\omega + 3m_\chi))). \tag{4.18}
\end{aligned}$$

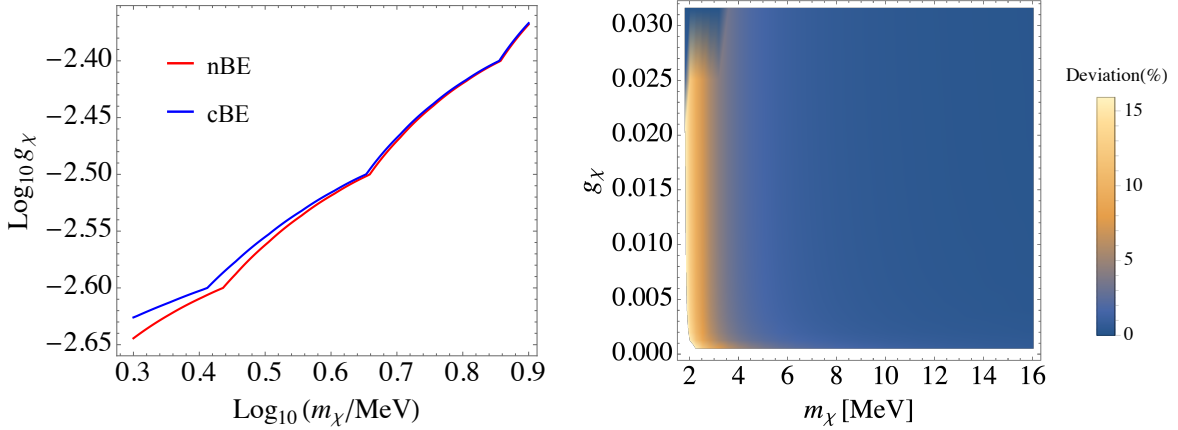


**Figure 3:** Left: Correct DM relic density for Case-1 (nBE) and Case-3 (cBE) in  $(m_\chi - g_\chi)$  plane. We fixed  $m_\phi = 1.2$  MeV. Right: the comparison of Case-1 and Case-3, the deviation is defined as  $(\Omega_\chi^{\text{cBE}} h^2 - \Omega_\chi^{\text{nBE}} h^2) / \Omega_\chi^{\text{cBE}} h^2$ .

In Fig. 3, we show the correct relic density in  $m_\chi - g_\chi$  plane. We use DRAKE [59] to compute the relic density in Case-1 (nBE) and Case-3 (cBE) in the left panel of Fig. 3. The red line corresponds to the correct relic density of Case-1; while the blue line corresponds to Case-3 with the early kinetic decoupling effect. We can find that the deviation happens for the small mass splitting between dark matter and mediator. When the dark matter becomes heavier than the mediator a lot, the two scenarios become degenerate. It can be seen in right panel the deviation (defined as  $(\Omega_\chi^{\text{cBE}} h^2 - \Omega_\chi^{\text{nBE}} h^2) / \Omega_\chi^{\text{cBE}} h^2$ ) can be at most 15%.

## 5 Conclusion

In this paper, we propose a flavor-specific scalar mediator model with only muon and down-quark coupling existing. These appear to be promising ways to explain the muon g-2 anomaly and the proton radius puzzle. The interaction with muon and down-quark causes observations in different experiments, which can constrain our model. The MeV mediator has loop-induced coupling with photons. Therefore it leads to observational phenomenologies in beam-dump

experiments such as E137 and supernova cooling. We also find that there is little parameter space left for  $g_\mu$  and  $g_d$ , implying that there is significant future discovery potential for our model from precision measurement on proton radius and other high-intensity frontiers such as NA62. To produce the right amount of thermal relics during cosmological evolution, we study all the possible modifications to the secluded dark matter. For early kinetic decoupling modification, the deviation of relic density can be as much as 10% level for MeV-scale dark matter. While for the bound state formation modification, it is negligible from consideration of the vacuum stability requirements and CMB constraint.

## Acknowledgements

Bin Zhu was supported by the National Natural Science Foundation of China under the grants No. 11805161, by the Natural Science Foundation of Shandong Province under the grants No. ZR2018QA007, by the Basic Science Research Program through the National Research Foundation of Korea (NRF) funded by the Ministry of Education, Science and Technology (NRF-2019R1A2C2003738), and by the Korea Research Fellowship Program through the NRF funded by the Ministry of Science and ICT (2019H1D3A1A01070937). Xuewen Liu was supported by the National Natural Science Foundation of China under the Grants No. 11947034 and No. 12005180, and by the Natural Science Foundation of Shandong Province under the Grant No. ZR2020QA083. This work is also supported by the Project of Shandong Province Higher Educational Science and Technology Program under Grants No. 2019KJJ007.

## References

- [1] MUON G-2 collaboration, *Final Report of the Muon E821 Anomalous Magnetic Moment Measurement at BNL*, *Phys. Rev. D* **73** (2006) 072003 [[hep-ex/0602035](#)].
- [2] PARTICLE DATA GROUP collaboration, *Review of Particle Physics*, *Phys. Rev. D* **98** (2018) 030001.
- [3] M. Davier, A. Hoecker, B. Malaescu and Z. Zhang, *Reevaluation of the hadronic vacuum polarisation contributions to the Standard Model predictions of the muon  $g - 2$  and  $\alpha(m_Z^2)$  using newest hadronic cross-section data*, *Eur. Phys. J. C* **77** (2017) 827 [[1706.09436](#)].
- [4] RBC, UKQCD collaboration, *Calculation of the hadronic vacuum polarization contribution to the muon anomalous magnetic moment*, *Phys. Rev. Lett.* **121** (2018) 022003 [[1801.07224](#)].
- [5] A. Keshavarzi, D. Nomura and T. Teubner, *Muon  $g - 2$  and  $\alpha(M_Z^2)$ : a new data-based analysis*, *Phys. Rev. D* **97** (2018) 114025 [[1802.02995](#)].
- [6] M. Davier, A. Hoecker, B. Malaescu and Z. Zhang, *A new evaluation of the hadronic vacuum polarisation contributions to the muon anomalous magnetic moment and to  $\alpha(m_Z^2)$* , *Eur. Phys. J. C* **80** (2020) 241 [[1908.00921](#)].
- [7] T. Aoyama et al., *The anomalous magnetic moment of the muon in the Standard Model*, [2006.04822](#).

- [8] MUON  $g - 2$  COLLABORATION collaboration, *Measurement of the positive muon anomalous magnetic moment to 0.46 ppm*, *Phys. Rev. Lett.* **126** (2021) 141801.
- [9] R. Pohl et al., *The size of the proton*, *Nature* **466** (2010) 213.
- [10] P.J. Mohr, B.N. Taylor and D.B. Newell, *CODATA Recommended Values of the Fundamental Physical Constants: 2006*, *Rev. Mod. Phys.* **80** (2008) 633 [[0801.0028](#)].
- [11] P.J. Mohr, D.B. Newell and B.N. Taylor, *CODATA Recommended Values of the Fundamental Physical Constants: 2014*, *Rev. Mod. Phys.* **88** (2016) 035009 [[1507.07956](#)].
- [12] W. Xiong et al., *A small proton charge radius from an electron-proton scattering experiment*, *Nature* **575** (2019) 147.
- [13] A. Beyer et al., *The Rydberg constant and proton size from atomic hydrogen*, *Science* **358** (2017) 79.
- [14] N. Bezginov, T. Valdez, M. Horbatsch, A. Marsman, A.C. Vutha and E.A. Hessels, *A measurement of the atomic hydrogen Lamb shift and the proton charge radius*, *Science* **365** (2019) 1007.
- [15] H. Fleurbaey, S. Galtier, S. Thomas, M. Bonnaud, L. Julien, F. Biraben et al., *New Measurement of the  $1S - 3S$  Transition Frequency of Hydrogen: Contribution to the Proton Charge Radius Puzzle*, *Phys. Rev. Lett.* **120** (2018) 183001 [[1801.08816](#)].
- [16] M. Mihovilović et al., *The proton charge radius extracted from the initial-state radiation experiment at MAMI*, *Eur. Phys. J. A* **57** (2021) 107 [[1905.11182](#)].
- [17] R. Essig et al. 10, 2013 [[1311.0029](#)].
- [18] B.P. Padley, K. Sinha and K. Wang, *Natural Supersymmetry, Muon  $g - 2$ , and the Last Crevices for the Top Squark*, *Phys. Rev. D* **92** (2015) 055025 [[1505.05877](#)].
- [19] J. Alexander et al., *Dark Sectors 2016 Workshop: Community Report*, 8, 2016 [[1608.08632](#)].
- [20] M. Battaglieri et al. 7, 2017 [[1707.04591](#)].
- [21] A. Das, T. Nomura, H. Okada and S. Roy, *Generation of a radiative neutrino mass in the linear seesaw framework, charged lepton flavor violation, and dark matter*, *Phys. Rev. D* **96** (2017) 075001 [[1704.02078](#)].
- [22] D. Sabatta, A.S. Cornell, A. Goyal, M. Kumar, B. Mellado and X. Ruan, *Connecting muon anomalous magnetic moment and multi-lepton anomalies at LHC*, *Chin. Phys. C* **44** (2020) 063103 [[1909.03969](#)].
- [23] R.T. D’Agnolo, D. Liu, J.T. Ruderman and P.-J. Wang, *Forbidden Dark Matter Annihilations into Standard Model Particles*, [2012.11766](#).
- [24] L. Su, W. Wang, L. Wu, J.M. Yang and B. Zhu, *Atmospheric Dark Matter and Xenon1T Excess*, *Phys. Rev. D* **102** (2020) 115028 [[2006.11837](#)].
- [25] S. Alekhin et al., *A facility to Search for Hidden Particles at the CERN SPS: the SHiP physics case*, *Rept. Prog. Phys.* **79** (2016) 124201 [[1504.04855](#)].
- [26] B. Batell, A. Freitas, A. Ismail and D. McKeen, *Flavor-specific scalar mediators*, *Phys. Rev. D* **98** (2018) 055026 [[1712.10022](#)].

- [27] B. Batell, A. Freitas, A. Ismail and D. McKeen, *Probing Light Dark Matter with a Hadrophilic Scalar Mediator*, *Phys. Rev. D* **100** (2019) 095020 [[1812.05103](#)].
- [28] G. Krnjaic, G. Marques-Tavares, D. Redigolo and K. Tobioka, *Probing Muonphilic Force Carriers and Dark Matter at Kaon Factories*, *Phys. Rev. Lett.* **124** (2020) 041802 [[1902.07715](#)].
- [29] G. Krnjaic, *Probing Light Thermal Dark-Matter With a Higgs Portal Mediator*, *Phys. Rev. D* **94** (2016) 073009 [[1512.04119](#)].
- [30] J.D. Bjorken, S. Ecklund, W.R. Nelson, A. Abashian, C. Church, B. Lu et al., *Search for neutral metastable penetrating particles produced in the slac beam dump*, *Phys. Rev. D* **38** (1988) 3375.
- [31] B. Döbrich, J. Jaeckel, F. Kahlhoefer, A. Ringwald and K. Schmidt-Hoberg, *ALPtraum: ALP production in proton beam dump experiments*, *JHEP* **02** (2016) 018 [[1512.03069](#)].
- [32] M.J. Dolan, T. Ferber, C. Hearty, F. Kahlhoefer and K. Schmidt-Hoberg, *Revised constraints and Belle II sensitivity for visible and invisible axion-like particles*, *JHEP* **12** (2017) 094 [[1709.00009](#)].
- [33] BNL-E949 collaboration, *Study of the decay  $K^+ \rightarrow \pi^+ \nu \bar{\nu}$  in the momentum region  $140 < P_\pi < 199$  MeV/c*, *Phys. Rev. D* **79** (2009) 092004 [[0903.0030](#)].
- [34] T. Bringmann and M. Pospelov, *Novel direct detection constraints on light dark matter*, *Phys. Rev. Lett.* **122** (2019) 171801 [[1810.10543](#)].
- [35] Y. Ema, F. Sala and R. Sato, *Light Dark Matter at Neutrino Experiments*, *Phys. Rev. Lett.* **122** (2019) 181802 [[1811.00520](#)].
- [36] Y.-S. Liu, D. McKeen and G.A. Miller, *Electrophobic Scalar Boson and Muonic Puzzles*, *Phys. Rev. Lett.* **117** (2016) 101801 [[1605.04612](#)].
- [37] X. Liu, Y. Li, T. Li and B. Zhu, *The light sgoldstino phenomenology: explanations for the muon  $(g - 2)$  deviation and KOTO anomaly*, *JHEP* **10** (2020) 197 [[2006.08869](#)].
- [38] NA62 collaboration, *Precision Measurement of the Ratio of the Charged Kaon Leptonic Decay Rates*, *Phys. Lett. B* **719** (2013) 326 [[1212.4012](#)].
- [39] R. Jackiw and S. Weinberg, *Weak interaction corrections to the muon magnetic moment and to muonic atom energy levels*, *Phys. Rev. D* **5** (1972) 2396.
- [40] V. Barger, C.-W. Chiang, W.-Y. Keung and D. Marfatia, *Proton size anomaly*, *Phys. Rev. Lett.* **106** (2011) 153001 [[1011.3519](#)].
- [41] D. Tucker-Smith and I. Yavin, *Muonic hydrogen and MeV forces*, *Phys. Rev. D* **83** (2011) 101702 [[1011.4922](#)].
- [42] G.A. Miller, *Non-Perturbative Lepton Sea Fermions in the Nucleon and the Proton Radius Puzzle*, *Phys. Rev. C* **91** (2015) 055204 [[1501.01036](#)].
- [43] M. Perelstein and Y.C. San, *Dark Matter as a Solution to Muonic Puzzles*, *Phys. Rev. D* **103** (2021) 035032 [[2009.09867](#)].
- [44] R. Bollig, W. DeRocco, P.W. Graham and H.-T. Janka, *Muons in supernovae: implications for the axion-muon coupling*, *Phys. Rev. Lett.* **125** (2020) 051104 [[2005.07141](#)].
- [45] J.L. Friar, *THE He-3 - H-3 CHARGE FORM-FACTOR AND THE He-3 COULOMB ENERGY*, *Nucl. Phys. A* **156** (1970) 43.



- [46] J.L. Friar and B.F. Gibson, *Coulomb Energies in S Shell Nuclei and Hypernuclei*, *Phys. Rev. C* **18** (1978) 908.
- [47] S.A. Coon and R.C. Barrett,  $\rho - \Omega$  Mixing in Nuclear Charge Asymmetry, *Phys. Rev. C* **36** (1987) 2189.
- [48] G.A. Miller, B.M.K. Nefkens and I. Slaus, *Charge symmetry, quarks and mesons*, *Phys. Rept.* **194** (1990) 1.
- [49] R.B. Wiringa, S. Pastore, S.C. Pieper and G.A. Miller, *Charge-symmetry breaking forces and isospin mixing in  $^8\text{Be}$* , *Phys. Rev. C* **88** (2013) 044333 [[1308.5670](#)].
- [50] H. Leeb and J. Schmiedmayer, *Constraint on hypothetical light interacting bosons from low-energy neutron experiments*, *Phys. Rev. Lett.* **68** (1992) 1472.
- [51] MINIBOONE DM collaboration, *Dark Matter Search in Nucleon, Pion, and Electron Channels from a Proton Beam Dump with MiniBooNE*, *Phys. Rev. D* **98** (2018) 112004 [[1807.06137](#)].
- [52] BELLE II collaboration, *Search for an Invisibly Decaying  $Z'$  Boson at Belle II in  $e^+e^- \rightarrow \mu^+\mu^-(e^\pm\mu^\mp)$  Plus Missing Energy Final States*, *Phys. Rev. Lett.* **124** (2020) 141801 [[1912.11276](#)].
- [53] NA62 collaboration, *Search for  $K^+$  decays to a muon and invisible particles*, [2101.12304](#).
- [54] T.-H. Yeh, K.A. Olive and B.D. Fields, *The impact of new  $d(p, \gamma)^3$  rates on Big Bang Nucleosynthesis*, *JCAP* **03** (2021) 046 [[2011.13874](#)].
- [55] H. An, M.B. Wise and Y. Zhang, *Strong CMB Constraint On P-Wave Annihilating Dark Matter*, *Phys. Lett. B* **773** (2017) 121 [[1606.02305](#)].
- [56] R. Onkala and K. Petraki, *Dark matter bound state formation via emission of a charged scalar*, *JHEP* **02** (2020) 036 [[1911.02605](#)].
- [57] T. Binder, K. Mukaida and K. Petraki, *Rapid bound-state formation of Dark Matter in the Early Universe*, *Phys. Rev. Lett.* **124** (2020) 161102 [[1910.11288](#)].
- [58] R. Onkala and K. Petraki, *Dark matter bound states via emission of scalar mediators*, *JHEP* **01** (2019) 070 [[1808.04854](#)].
- [59] T. Binder, T. Bringmann, M. Gustafsson and A. Hryczuk, *DRAKE: Dark matter Relic Abundance beyond Kinetic Equilibrium*, [2103.01944](#).